

# PCCP

Accepted Manuscript



This is an *Accepted Manuscript*, which has been through the Royal Society of Chemistry peer review process and has been accepted for publication.

*Accepted Manuscripts* are published online shortly after acceptance, before technical editing, formatting and proof reading. Using this free service, authors can make their results available to the community, in citable form, before we publish the edited article. We will replace this *Accepted Manuscript* with the edited and formatted *Advance Article* as soon as it is available.

You can find more information about *Accepted Manuscripts* in the [Information for Authors](#).

Please note that technical editing may introduce minor changes to the text and/or graphics, which may alter content. The journal's standard [Terms & Conditions](#) and the [Ethical guidelines](#) still apply. In no event shall the Royal Society of Chemistry be held responsible for any errors or omissions in this *Accepted Manuscript* or any consequences arising from the use of any information it contains.

## ARTICLE

# Optimization of Amorphous Silicon Double Junction Solar Cells for an Efficient Photoelectrochemical Water Splitting Device Based on Bismuth Vanadate Photoanode

Cite this: DOI: 10.1039/x0xx00000x

Received 00th December 2013,  
Accepted 00th December 2013

DOI: 10.1039/x0xx00000x

[www.rsc.org/](http://www.rsc.org/)Lihao Han,<sup>\*a</sup> Fatwa F. Abdi,<sup>b,c</sup> Paula Perez Rodriguez,<sup>a</sup> Bernard Dam,<sup>b</sup> Roel van de Krol,<sup>b,c</sup> Miro Zeman<sup>a</sup> and Arno H.M. Smets<sup>a</sup>

A photoelectrochemical water splitting device (PEC-WSD) was designed and fabricated based on cobalt-phosphate-catalysed and tungsten-gradient-doped bismuth vanadate (W:BiVO<sub>4</sub>) as the photoanode. A simple and cheap hydrogenated amorphous silicon (a-Si:H) double junction solar cell has been used to provide additional bias. The advantage of using thin film silicon (TF-Si) based solar cells is that this photovoltaic (PV) technology meets the crucial requirements for the PV component in PEC-WSDs based on W:BiVO<sub>4</sub> photoanodes. TF-Si PV devices are stable in aqueous solutions, are manufactured in simple and cheap fabrication processes and their spectral response, voltage and current density show an excellent match with the photoanode. This paper is mainly focused on the optimization of the TF-Si solar cell in reference to the remaining solar spectrum transmitted through the W:BiVO<sub>4</sub> photoanode. The current matching between the top and bottom cells are studied and optimized by varying the thickness of the a-Si:H top cell. We support the experimental optimization of the current balance between the two sub-cells with simulations of the PV devices. In addition, the impact of the light induced degradation of the a-Si:H double junction, the so-called Staebler-Wronski Effect (SWE), on the performance of the PEC-WSD has been studied. The light soaking experiments on the a-Si:H/a-Si:H double junctions over 1000 hours show that the efficiency of a stand-alone a-Si:H/a-Si:H double junction cell is significantly reduced due to the SWE. Nevertheless, the SWE has a significant smaller effect on the performance of the PEC-WSD.

## 1. PEC-WSDs based on BiVO<sub>4</sub>

A photoelectrochemical water splitting device (PEC-WSD) provides an attractive route in utilizing sunlight to split water into hydrogen (H<sub>2</sub>) and oxygen (O<sub>2</sub>). H<sub>2</sub> can then be directly used as a fuel in a combustion engine, or as an intermediate to form hydrocarbons. Electrodes based on metal oxide semiconductors have been the focus of many studies as potential PEC-WSDs, mainly due to their stability in aqueous solutions, easy synthesis, and low costs. One of the most promising metal oxide semiconductors is bismuth vanadate (BiVO<sub>4</sub>).<sup>1,2</sup> In the monoclinic phase, BiVO<sub>4</sub> is a photoactive *n*-type semiconductor,<sup>3,4</sup> and it is stable in aqueous solution with pH values between 3 and 11.<sup>5</sup> Theoretically, BiVO<sub>4</sub> can generate a photocurrent of ~7.5 mA·cm<sup>-2</sup> under an AM1.5 solar

spectrum (1000 W·m<sup>-2</sup>), assuming that all photons with energies higher than the bandgap (2.4 eV<sup>6</sup>) are absorbed and contribute to the O<sub>2</sub> generation at the surface.

Early efforts in employing BiVO<sub>4</sub> as the photoanode material, however, have been hampered by low efficiencies, resulting in AM1.5 photocurrents lower than 1 mA·cm<sup>-2</sup> at 1.23 V vs. reversible hydrogen electrode (RHE).<sup>7-11</sup> In the last couple of years, BiVO<sub>4</sub> performance has been improved significantly by modifying the material with O<sub>2</sub> evolution catalysts.<sup>2,12-19</sup> The remaining technological bottleneck is the substantial additional bias potential that needs to be applied in order to draw a reasonable photocurrent. Reducing or eliminating this bias is a challenge for nearly all visible-light absorbing PEC materials, such as BiVO<sub>4</sub>, α-Fe<sub>2</sub>O<sub>3</sub>,<sup>20</sup> WO<sub>3</sub>,<sup>21</sup> and Ta<sub>3</sub>N<sub>5</sub>.<sup>22</sup> The

demonstration of AM1.5 photocurrents higher than  $2 \text{ mA}\cdot\text{cm}^{-2}$  for  $\text{BiVO}_4$  requires an external bias higher than 1 V. This is usually supplied by an external voltage source (e.g. potentiostat), which significantly reduces the overall solar-to-hydrogen conversion efficiency ( $\eta_{STH}$ ).<sup>23</sup>

An elegant solution to the problem is to employ a Z-scheme configuration (named after the shape of energy diagram), by combining a photoelectrode material with a photovoltaic solar cell.<sup>24</sup> In this configuration, the solar cell is placed at the back of the photoelectrode. Using the light transmitted through the photoelectrode, the solar cell can supply the bias voltage needed by the photoelectrode as reported in various publications.<sup>25,26</sup> The solar cells integrated in PEC-WSDs range from dye-sensitized solar cells (DSSCs)<sup>27</sup> and GaAs *p-n* junction solar cells<sup>28</sup> to more sophisticated AlGaAs/Si solar cell configurations.<sup>29</sup> The choice of PV material is determined by two competing requirements, one related to cost reduction and one related to high conversion efficiencies. Very cheap solar cells usually have lower conversion efficiencies, while the high conversion efficiencies can only be achieved with expensive solar cells.

In a recent publication, we have demonstrated that a W:BiVO<sub>4</sub> photoanode powered by an a-Si:H tandem cell could give a solar-to-hydrogen efficiency of 4.9%, which is currently the highest value ever reported for a water splitting device based on a metal oxide photoelectrode.<sup>30</sup> In this paper, we will discuss the advantages of using a-Si:H tandem solar cells for PEC-WSDs based on W:BiVO<sub>4</sub> photoanodes, and will focus on the optimization of the solar cell in reference to the solar spectrum transmitted to the W:BiVO<sub>4</sub> based photoelectrode. We demonstrate that the light induced degradation of the a-Si:H solar cell, the so-called Staebler-Wronski Effect (SWE),<sup>31</sup> when integrated in a PEC-WSD has a smaller impact on the  $\eta_{STH}$  compared to the  $\eta_{STH}$  of a stand-alone a-Si:H/a-Si:H double junction PV device.

## 2. Why a-Si:H/a-Si:H tandem cells?

In this paper, we are still using platinum (Pt) as the counter electrode in the solution for an efficient H<sub>2</sub> evolution. However, in the long term strategy, the expensive Pt counter electrode has to be replaced by a cheaper metal and integrated at the back contact of the solar cell. This requires the photovoltaic cell to be immersed in water, so the first requirement for the PV cell in the PEC-WSD is that it should be stable in aqueous electrolytes. Silicon (Si) has been chosen as it is the most resistant PV material in aqueous environments. This allows the use of cheaper encapsulation materials than more sensitive PV materials, such as chalcogenides and III-V semiconductors. In addition, the same reasons why Si is the most dominant material in the PV industry apply to PEC-WSD as well. Si is earth-abundant, non-toxic, environmentally sustainable, relatively low-cost and widely investigated.

The second requirement is related to the transmittance of the solar spectrum through the photoanode component of the PEC-WSD. The maximum power point (MPP) of a stand-alone PV device is generally optimized in reference to the standard AM1.5 ( $1000 \text{ W}\cdot\text{m}^{-2}$ ) solar spectrum. In contrast, the PV cell in the PEC-WSD has to be optimized and work efficiently under illumination with AM1.5 sunlight that is filtered by the components at the front side: the quartz-window of the water tank, electrolyte, catalyst layer, photoanode films and F-doped SnO<sub>2</sub> (FTO) substrate of the device (as depicted in Figure 1 (a)). This transmitted spectrum (TS), shown by the yellow curve in Figure 1 (b), is missing most of the blue spectral region ( $\lambda < 450 \text{ nm}$ ) and contains around 60% of the irradiation of the AM1.5 spectrum in the red part ( $\lambda > 550 \text{ nm}$ ) (as depicted by the blue dash curve).

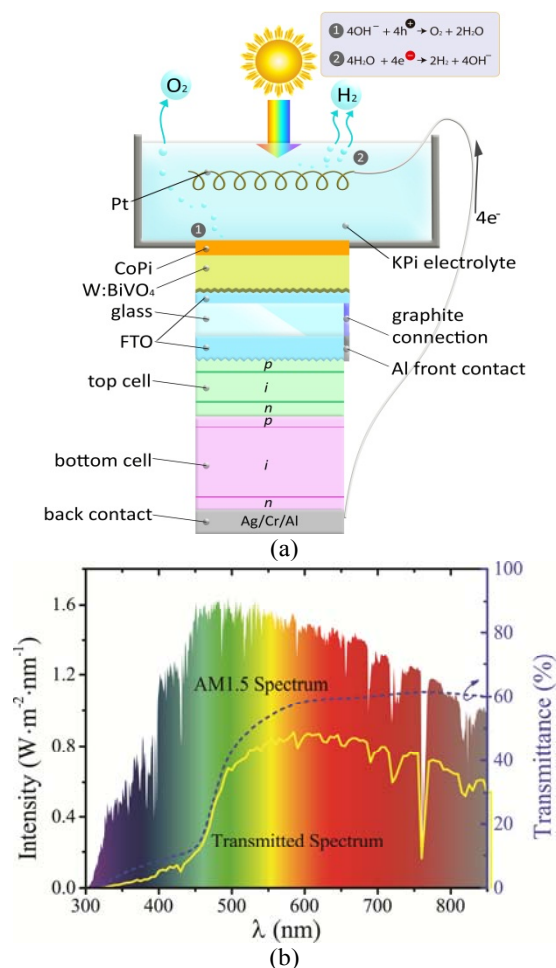


**Figure 1** The cross-section sketch of the photoelectrochemical water splitting device (PEC-WSD) demonstrated in this paper (a). The AM1.5 spectrum and the photoanode modified spectrum (left axis) and the transmittance spectrum (right axis) (b).

The third requirement for the PV cell is that its *j-V* characteristics should match the *j-V* curve of the photoanode. In our earlier work, an AM1.5 photocurrent density (*j*) of  $3.6 \text{ mA}\cdot\text{cm}^{-2}$  for a cobalt-phosphate-catalysed (CoPi) BiVO<sub>4</sub>-based

photoanode at 1.23 V vs. RHE was reported.<sup>19,30</sup> This remarkably high photocurrent for a material deposited using a low-cost and easily scalable spray pyrolysis process was achieved by introducing a gradient dopant profile of tungsten (W) in BiVO<sub>4</sub> to form a stack of homojunctions. This results in an enhanced internal electric field. This field greatly increases the charge separation efficiency, which was shown to be the main limiting factor for the performance of these spray-deposited BiVO<sub>4</sub> photoelectrodes.<sup>1</sup> The operating point (OP) of the PEC-WSD is determined by the intersection point of the *j*-*V* curve of the solar cells and that of photoanode device. For optimal performance, the OP has to be at a voltage as high as possible in order to get a sufficient bias potential to drive the surface reactions. Since the *j* of the photoanode levels off at *V* ≥ 1 V, it is more efficient if the *V*<sub>OP</sub> ≥ 1 V. This implies that the PV component needs to deliver an open-circuit voltage *V*<sub>OC</sub> ≥ 1.5 V, whereas *j* has to be matched with that of the photoanode. To obtain PV devices with *V*<sub>OC</sub> ≥ 1.5 V, options are limited to the implementation of multi-junction PV devices based on TF-Si or III-V materials. In this paper we do not consider III-V semiconductor materials as they suffer from both instability in aqueous environments and high costs. Typical materials used in TF-Si junctions are a-Si:H, amorphous silicon-germanium (a-SiGe:H) and nanocrystalline silicon (nc-Si:H). The band gaps of these materials determine the range of *V*<sub>OC</sub> that can be achieved in the corresponding junction, i.e. *V*<sub>OC,a-Si:H</sub> = 0.8-1.0 V, *V*<sub>OC,a-SiGe:H</sub> = 0.5-0.6 V and *V*<sub>OC,nc-Si:H</sub> = 0.48-0.6 V. Consequently, in view of the required *V*<sub>OC</sub> ≥ 1.5 V for the BiVO<sub>4</sub> photoanode, the PV device configurations are limited to an a-Si:/a-Si:H double junction or a triple junction devices (e.g., a-Si:H/a-Si:H/a-SiGe:H, a-Si:H/a-SiGe:H/a-SiGe:H, a-Si:H/nc-Si:H/nc-Si:H). The individual junctions in these multi-junction configurations have to deliver a *j* value of 7.5 mA•cm<sup>-2</sup> in reference to the TS to achieve the theoretical maximum  $\eta_{STH}$  of 9.2%.

In this contribution, we focus on the a-Si:H/a-Si:H double junction device instead of a triple junction device. The PV component of PEC-WSD is required to have a *V*<sub>OC</sub> as high as possible and a *j* value as high as possible when illuminated by the photons transmitted through the photoanode. These are competing parameters if we consider the double and triple junction. A triple junction has the advantage of a high *V*<sub>OC</sub>, but its short-circuit current density (*J*<sub>SC</sub>) is limited when the incident light is filtered by the photoanode. Due to the spectral overlap of the photoanode with the top cell, the triple junction can only deliver a maximum *J*<sub>SC</sub> of 3.8 mA•cm<sup>-2</sup> theoretically (this value is estimated according to the integration of the transmitted spectrum through the photoanode, assuming all the photons are converted into electron hole pairs and the current density is evenly distributed among all the three junctions). In contrast, the double junction cell generates a more moderate *V*<sub>OC</sub>, but has a much higher maximum theoretical *J*<sub>SC</sub> of 5.8 mA•cm<sup>-2</sup> when placed behind the photoanode. Since the *V*<sub>OC</sub> is sufficiently high to drive the W:BiVO<sub>4</sub> photoanode, the double junction is the most logical approach. Furthermore, it has

several advantages over the triple junction device. The total layer thickness of the double junction cell is significantly thinner than that of the triple junction device based on nc-Si:H material. The total amount of the layers in the double junction cell is less than that of the triple junctions and the deposition time is also much shorter. Therefore, it is the cheapest solution for this type of PEC-WSD. In addition, the tandem cell allows much more flexibility than the triple-junction cell for equally distributing the current density over both sub-cells by varying the film thicknesses or bandgap of the both junctions. Furthermore, at applied bias voltages larger than the typical value of redox potential of water ~1.23 V, the current density of the photoanode tends to saturate. The gain in  $\eta_{STH}$  by boosting the voltage of the solar cell above 2 V by using an additional thick bottom cell in a triple junction is therefore minimal. In view of all the above issues, the a-Si:H/a-Si:H device is the most straightforward option to meet the requirement for the PEC-WSD based on CoPi-catalysed gradient-doped W:BiVO<sub>4</sub>.

### 3. Experiment

The a-Si:H/a-Si:H solar cells were deposited in a multi-chamber tool equipped with radio frequency plasma enhanced chemical vapour deposition (RF-PECVD) reactors. Solar cells were deposited on 2.5 cm × 10 cm ASAHI VU-type substrates (~600 nm thick textured FTO on glass), which were kept at temperature of 170 °C during the TF-Si deposition. Before the deposition of TF-Si films, a stripe of 300 nm thick aluminium (Al) was coated near the edge of the ASAHI VU-type substrates using a Provac evaporator in a rotation mode. This Al stripe acts as the front contact of the tandem cell.

A boron-doped amorphous silicon carbide (a-SiC:H(B)) layer was deposited as *p*-layer. A very thin intrinsic a-SiC:H buffer layer was deposited between *p*- and a-Si:H *i*-layer to achieve higher values for *V*<sub>OC</sub>. The *n*-layer of the top cell is a single layer of phosphorus-doped nanocrystalline silicon oxide (nc-SiO<sub>x</sub>:H(P)) whereas the *n*-layer of the bottom cell is a double layer of nc-SiO<sub>x</sub>:H(P) and phosphorus-doped hydrogenated amorphous silicon (a-Si:H(P)). The *n*-type nc-SiO<sub>x</sub>:H(P) material has the advantage of lower parasitic absorption losses and better reflection performance in reference to the conventional *n*-type a-Si:H(P) with a higher refractive index (*n*).

Three layers of Ag/Cr/Al were evaporated on the *n*-type nc-SiO<sub>x</sub>:H(P) area as the back contact. The Al layer prevents the oxidation of the Ag layer, whereas the Cr interlayer avoids mixing of Ag and Al in post-deposition anneal treatments. All metal back contacts have an area of 1 cm × 1 cm. The cross-section sketch of the solar cell structure is shown in Figure 1 (a).

In this work, the thickness of the a-Si:H *i*-layer has been varied to optimize the performance of the solar cell. Three a-Si:H/a-Si:H tandem solar cells with different thicknesses of the top *i*-

layer (50 nm, 75 nm, 100 nm) were deposited, while the thickness for the bottom *i*-layer of 350 nm was kept the same for all three cells. In this paper we refer to these tandem cells as ‘thin cell’ (*i*-layer in top cell is 50 nm), ‘medium cell’ (*i*-layer in top cell is 75 nm) and ‘thick cell’ (*i*-layer in top cell is 100 nm).

The gradient-doped W:BiVO<sub>4</sub> was synthesized by spray pyrolysis on a piece of TEC-15 FTO substrate, and the fabrication procedure was reported in our previous publication.<sup>30</sup> PEC characterization was performed under a two-electrode configuration in 0.1 M (mol/L) KPi (pH ~7) aqueous solution as the electrolyte and Pt coil as the counter electrode.

The integrated PEC-WSDs were fabricated with the photoanode on the upper side of the glass substrate and an optimized solar cell at the bottom side of the glass substrate. Using the same substrate for both the spray pyrolysis technique on one side and RF-PECVD on the other side, might lead to cross-contamination of the solar cell and photoanode processing. Therefore, a more practical option is to process the photoanode and PV part on different glass substrates, which are subsequently connected back-to-back using transparent glue at the non-processed sides. The FTO window layer of the solar cell was connected to the FTO of the photoanode using a wire as illustrated in Figure 1 (a). The back contact of the solar cell was connected to the Pt counter electrode.

A PASAN flash AM1.5 spectrum solar simulator was used to measure the *j*-*V* characteristics of solar cells under standard test conditions. Using the flash simulator, a constant temperature of 25 °C on the surface of the solar cells during the measurement was guaranteed. In addition, an accurate illumination area was ensured by using a black mask to rule out possible contribution of contactless areas. During the flash measurement, a reference monitoring photodiode is used to calibrate the average intensity of the AM1.5 spectrum. The optical thickness and properties of the various films are determined using reflection and transmission measurements on each single layer. These layers were separately processed as single layers on flat glass substrates. The thickness of each film was determined using an optical model based on a Tauc-Lorentz oscillator as defined in SCOUT program.<sup>32</sup>

The external quantum efficiency (EQE) spectrum of solar cells indicates the fraction of photons at a certain wavelength that results in collected electrons at the contacts. It is not straightforward to measure the EQE of individual top and bottom cells as well as that of the total double junction solar cells. In this work, the device was illuminated by two different types of LEDs during the EQE measurement, respectively: red ( $\lambda = 632$  nm) LEDs to saturate the bottom cell and measure the top cell; blue LEDs ( $\lambda = 397$  nm) to saturate the top cell and measure the bottom cell. A problem in achieving a solely biased top cell or bottom cell is the fact that both junctions have the same absorber layers with in principal the same spectral

response. Light biasing the top cell is straightforward by using blue light, as the blue light is fully absorbed in the top cell. However, the bottom cell has to be biased by red light, which is also partly absorbed by the top cell. The intensity of the red LEDs is increased such that only the bottom cell is close to saturation (so no saturation of the top cell).

In this paper, we use two types of EQE spectra. The first type is the standard  $EQE_{AM1.5}$ , which is used to determine the  $J_{SC, AM1.5}$  out of the spectral photon flux  $\Phi_{AM1.5}$  under the standard solar spectrum of AM1.5 (1000 W·m<sup>-2</sup>):

$$J_{SC, AM1.5} = e \int \Phi_{AM1.5}(\lambda) EQE_{AM1.5}(\lambda) d\lambda \quad (1)$$

The second type of EQE spectra is referred to as  $EQE_{TS}$  which represents the spectral response of the PV component in which the optical losses due to the front photoanode and its supporting layers is included:

$$EQE_{TS}(\lambda) = T(\lambda) EQE_{AM1.5}(\lambda) \quad (2)$$

where  $T(\lambda)$  presents the transmittance of the photoanode component (Figure 1(b)). With

$$\Phi_{TS}(\lambda) = \Phi_{AM1.5}(\lambda) T(\lambda) \quad (3)$$

this gives the following expression for the short circuit density  $J_{SC, TS}$  of the PV device after the photoanode becomes

$$\begin{aligned} J_{SC, TS} &= e \int \Phi_{TS}(\lambda) EQE_{AM1.5}(\lambda) d\lambda \\ &= e \int \Phi_{AM1.5}(\lambda) T(\lambda) EQE_{AM1.5}(\lambda) d\lambda \\ &= e \int \Phi_{AM1.5}(\lambda) EQE_{TS}(\lambda) d\lambda \end{aligned} \quad (4)$$

and it is smaller than the  $J_{SC, AM1.5}$  value.

The potential of the working electrode (diameter 6 mm) was controlled by a potentiostat (EG&G PAR 283) and an immersed Pt wire was used as the counter electrode. White light photocurrent measurements were performed under simulated AM1.5 solar illumination (1000 W·m<sup>-2</sup>) with a NEWPORT Sol3A Class AAA solar simulator (type 94023A-SR3). Electrical contact to the sample was made using a silver wire and graphite paste. For the combined PEC-WSD, *j* was monitored by a digital multimeter (KEITHLEY 2001). It should be pointed out that the photoanode performance is very sensitive to the blue (and UV) spectrum, therefore, the measured *j* is highly sensitive to the differences in the shape of the blue spectral part between the various solar simulators (xenon vs. tungsten). This requires the solar simulator to be calibrated during the various measurements to minimize the possible spectrum mismatching with AM1.5 spectrum. During the *j*-*t* curve measurement of the PEC-WSD, the external power applied to the Class AAA solar simulator is real-time controlled to guarantee an irradiance equal to standard test conditions (1000 W·m<sup>-2</sup>).

#### 4. Solar Cell Optimization

In this section, we optimize the current matching of the a-Si:H/a-Si:H double junctions and consequently the  $\eta_{STH}$  of the PEC-WSD. First, as a reference, we compare the  $EQE_{AMI.5}$  of the a-Si:H/a-Si:H double junctions with a single junction a-Si:H solar cell with an  $i$ -layer thickness of 350 nm (corresponding to the bottom cell of the a-Si:H/a-Si:H double junction). The  $EQE_{AMI.5}$  of the single junction a-Si:H solar cell shows that it utilizes the AM1.5 solar spectrum in the range of 300 nm up to 800 nm (blue curve in Figure 2 (a)) better than that of the double junctions. In the a-Si:H/a-Si:H double junction structure, the spectral utilization of the AM1.5 solar spectrum is distributed over the top cell ( $300 \text{ nm} < \lambda_{abs} < 750 \text{ nm}$ ) and the thicker (350 nm) bottom cell ( $400 \text{ nm} < \lambda_{abs} < 800 \text{ nm}$ ). The sum of the top and the bottom cell results in a slightly smaller  $EQE_{AMI.5}$  in the spectral range of  $\lambda > 450 \text{ nm}$  in reference to the single junction solar cell. This lower response is explained as the additional doped layers between the top and bottom junctions, which are logically lacking in the single junction. These layers result in additional parasitic losses and reflection losses back in to the top cell due to the nc-SiO<sub>x</sub>:H  $n$ -layer with low refractive index values. The double junction with the highest total spectral utilization is the thick cell (green curves in Figure 2 (a)), which shows a slight enhancement of the EQE in the 400-550 nm range. This indicates that a thick top cell leads to a reduction of the parasitic absorption losses in the  $n$ -doped and  $p$ -doped layer between the top and bottom cell. The blue response (300-450 nm) shows a slightly lower  $EQE_{AMI.5}$  for the single junction compared to the double junctions. Both configurations have the same  $p$ -layer, so the difference in blue response is not based on parasitic absorption losses in the supporting layers.

It is important to note that we have ruled out the possibility of an artefact of the EQE measurement approach. In practice, by light biasing one of the sub-cells in the double junction under  $V = 0 \text{ V}$  conditions, the light-biased sub-cell puts a reverse bias of approximately  $-0.65 \text{ V}$  (an estimated voltage between  $V_{OC}$  and  $V_{MPPT}$  of one a-Si:H sub-cell) on the non-light-biased cell. To study the extent of this effect, the EQE spectral response of the single junction solar cell was measured under an intentionally reverse bias of  $-0.65 \text{ V}$  as well. As illustrated in Figure 2 (a) (magenta coloured curve), the EQE curve somewhat increases in the whole measured wavelength range, but its blue response in the  $\lambda < 450 \text{ nm}$  range is still lower than for the double junction. Consequently, the origin of the improved collection in the blue spectrum is believed to be a result of the larger internal electric field as a result of the much thinner top cells in the double junctions in reference to the rather thick single junction. The thicker single junction results in a smaller internal electric field and less effective collection of the close to the  $p$ - $i$  interface photo-excited charge carriers. The single junction under reverse bias results in small increase in the current of  $\Delta J_{SC} = 0.3 \text{ mA}\cdot\text{cm}^{-2}$ . This implies that the determined  $J_{SC}$  of sub-cells in the tandem cell using EQE and light biasing can lead to a maximum systematic overestimation of the current of

$\Delta J_{SC} / J_{SC} = 1.7\%$ , due to mutual voltage biasing between the sub-cells.

Next, the spectral matching of the double junctions with the PEC-WSD is analysed. The  $EQE_{TS}$  of the three devices in reference to the spectrum transmitted through the photoanode structure CoPi/BiVO<sub>4</sub>/FTO/glass is determined by measuring  $EQE_{AMI.5}(\lambda)$  and  $T(\lambda)$  of the photoanode (using Equation (2)). The resulting  $EQE_{TS}$  are shown in Figure 2 (b). The same  $EQE_{TS}(\lambda)$  spectra have been directly measured by placing the photoanode structure as a ‘high-pass filter’ between the monochromator and the solar cell during the EQE measurement. The  $T(\lambda)$  of the photoanode has a relatively low transmission of  $\sim 10\%$  in the blue region ( $\lambda < 450 \text{ nm}$ ), whereas it has a moderate transmission of  $\sim 60\%$  in the red region. Consequently, the  $EQE_{TS}(\lambda)$  of the solar cell is significantly reduced in the blue range and therefore affects the top cell the most.

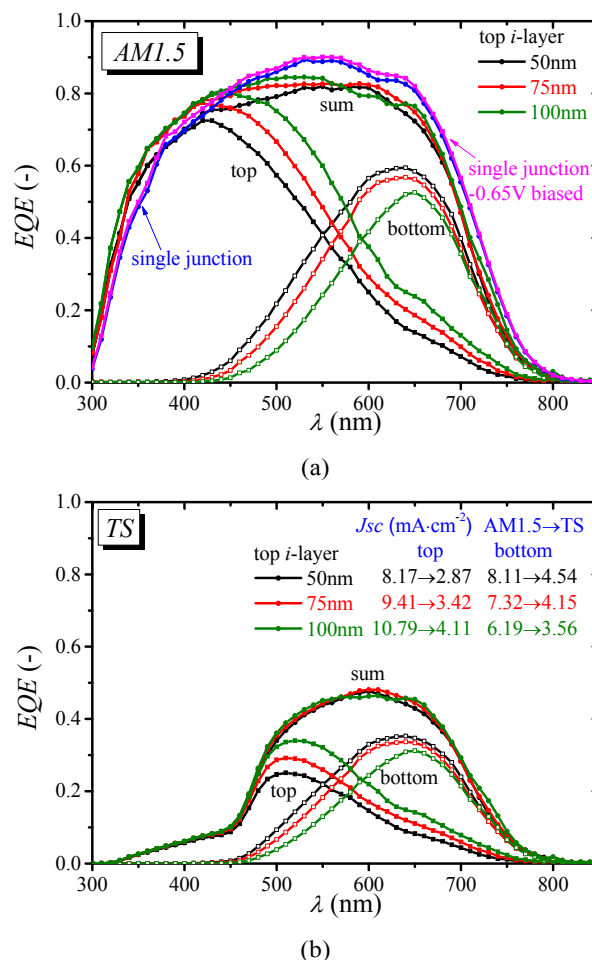


**Figure 2** EQE spectra in the series of the top  $i$ -layer thickness (black: thin cell, red: medium cell, green: thick cell), compared with that of single junction a-Si:H solar cell (blue and magenta) (a); EQE spectra of the three tandem PV cells calculated under the transmitted spectrum through the photoanode (b)

Additional validation of the EQE measurements is obtained by simulating the performance of the a-Si:H/a-Si:H solar cell

structures using the in-house developed Advance Semiconductor Analysis (ASA) software.<sup>33</sup> A semiconductor model of the a-Si:H/a-Si:H solar cell is built in ASA, and the measured wavelength dependent  $n(\lambda)$  and  $k(\lambda)$  (extinction coefficient) values have been used as the optical input data for the simulation. The simulations have been performed for the three tandem cells: the thin cell, the medium cell and the thick cell. The simulated  $EQE_{AM1.5}$  and  $EQE_{TS}$  of each cell are depicted in Figure 3 (a) and (b), respectively. The simulated EQE spectra closely resembles the measured  $EQE_{AM1.5}$  and  $EQE_{TS}$  as shown in Figure 2 (a) and (b), implying that our approach of measuring  $EQE_{AM1.5}$  and  $EQE_{TS}$  is validated.

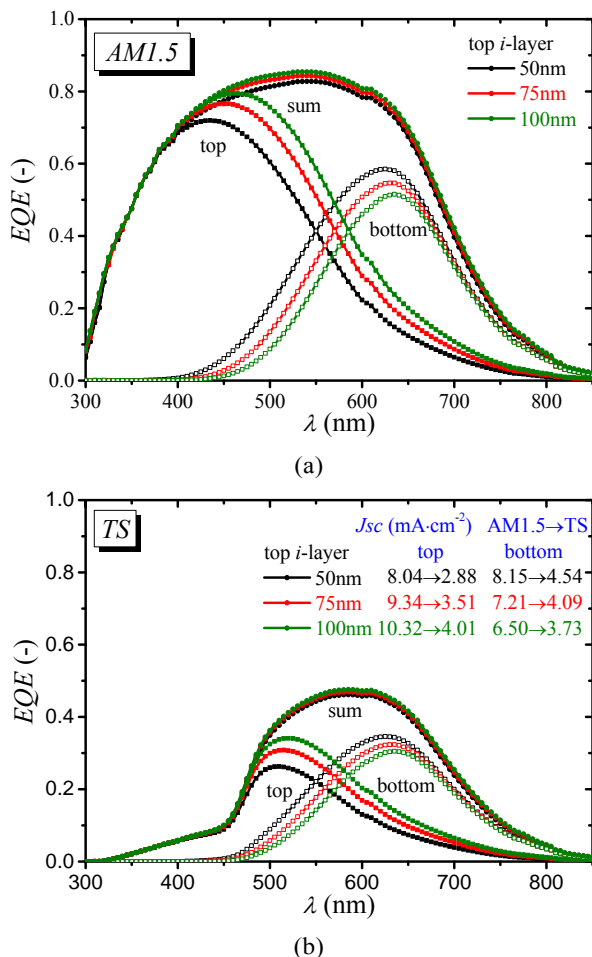


**Figure 3** ASA simulation of EQE spectra in the series of the top  $i$ -layer thickness (black: thin cell, red: medium cell, green: thick cell), compared with that of single junction a-Si:H solar cell (blue and magenta) (a); and under the transmitted spectrum through the photoanode (b)

The optimum current matching between the top and bottom cell depends on the employed spectrum. Figure 4 shows both the short circuit densities  $J_{SC,AM1.5}$  and  $J_{SC,TS}$  of the top and bottom cell for the three a-Si:H/a-Si:H double junctions for the AM1.5 solar spectrum and the TS through the photoanode structure, respectively. The solid and dashed lines indicate the result from experiment and simulation, respectively, which are in excellent

agreement. For the AM1.5 spectrum the double junction is limited by the  $J_{SC,AM1.5}$  of the 350 nm thick bottom cell. The thin cell shows an excellent current matching between the top and bottom cells, whereas the medium and thick cells are bottom-limited. The situation is different when part of the spectrum is filtered by the photoanode. Since the photoanode mainly absorbs the blue light,  $J_{SC,TS}$  becomes top-limited for the thin and medium solar cells. The data in Figure 4 show that an  $\sim 89$  nm top cell is perfectly current-matched with a 350 nm thick  $i$ -layer in this a-Si:H/a-Si:H device.

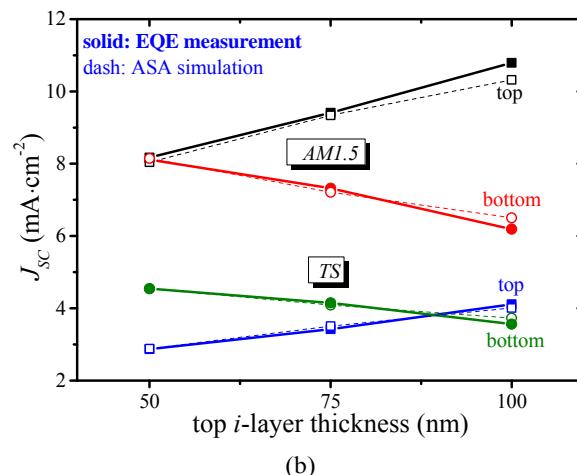


**Figure 4** The  $J_{SC}$  of the reported a-Si:H/a-Si:H cell under the standard AM1.5 spectrum illumination (solid black & red) and under the transmitted spectrum (TS) through the photoanode (solid blue & green); compared with those values from the ASA simulation (dash)

Figure 5 illustrates the external parameters of the tandem solar cells,  $V_{OC,AM1.5}$ ,  $J_{SC,AM1.5}$ , fill factor ( $FF_{AM1.5}$ ), efficiency ( $\eta_{PV,AM1.5}$ ) under standard AM1.5 illumination (black squares) and  $V_{OC,TS}$ ,  $J_{SC,TS}$ ,  $FF_{TS}$ ,  $\eta_{TS}$ , under illumination of spectrum transmitted through the photoanode (red circles).

As discussed above, the  $J_{SC,TS}$  of the PV device decreases significantly in reference to  $J_{SC,AM1.5}$  when the cell is positioned after the photoanode material. The various  $V_{OC}$  values remain roughly constant for the three devices. Slightly lower  $V_{OC,TS}$  values are measured for the transmitted spectrum due to the weak dependence of the  $V_{OC}$  on the current density<sup>34</sup>

$$V_{OC} = \frac{kT}{q} \times \ln\left(\frac{J_{SC}}{J_0} + 1\right) \quad (5)$$

When illuminated by the standard AM1.5 solar spectrum, the current-matched thin solar cell results in the highest  $J_{SC,AM1.5}$  and consequently the highest  $V_{OC,AM1.5}$ . But when the double junction is shaded by the photoanode, the  $J_{SC,TS}$  of the thin solar cell drops the most due to the heavily current-limited top cell. The highest  $J_{SC,TS}$  is obtained for the double junction with the thickest top cell, as it is the configuration closest to the optimum condition for current matching ( $i$ -layer thickness of  $\sim 89$  nm in top cell). The  $\eta_{STH}$  for this device, in which no external bias is applied, is defined as<sup>35</sup>

$$\eta_{STH} = J_{OP}(\text{mA}\cdot\text{cm}^{-2}) \times \frac{1.23\text{V}}{100\text{mW}\cdot\text{cm}^{-2}} \times 100\% \quad (6)$$

The value of 1.23 V is the chemical potential needed to split the H<sub>2</sub>O molecule,  $J_{OP}$  is the current density at the operating point, and 100 mW·cm<sup>-2</sup> (or 1000 W·m<sup>-2</sup>) is the average intensity of AM1.5 spectrum. At first glance it might be surprising to see that the thin and medium cells have higher  $\eta_{STH}$  values than their PV component  $\eta_{TS}$  values (the efficiency of the tandem solar cell operating in the spectrum which is transmitted from the photocathode). It is important to realize that for  $\eta_{TS}$ , the majority of the energy in blue part of the AM1.5 solar spectrum does not contribute to generating voltage and current, whereas the energy in this spectral part does contribute to the performance  $\eta_{STH}$  of the PEC-WSD.

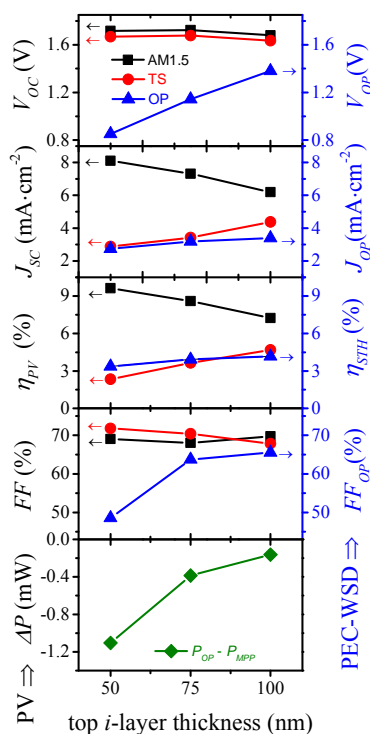


**Figure 5** The external electrical properties of a-Si:H/a-Si:H solar cells in the series of top *i*-layer thickness illuminated by the standard AM1.5 solar spectrum (black square) and by the photoanode transmitted spectrum (TS) (red circle), the operating point (OP) for PEC-WSDs (blue triangle), and the power mismatching between the OP and the corresponding maximum power point (MPP) (green diamond).

In Figure 6, the  $j$ - $V$  curves of the BiVO<sub>4</sub> photoanode structure and the a-Si:H/a-Si:H double junctions are illustrated. It is obvious that the thick solar cell results in the largest power at its OP, in spite of the fact that its  $V_{OC}$  is slightly lower compared to the other two cells. Combination of the PEC cell and the PV solar cell would result in a  $\eta_{STH}$  of 4.2%. The voltage  $V_{OP}$ , current density  $J_{OP}$  and  $\eta_{STH}$  at OP are presented by the blue triangles in Figure 5 (right-side axis), respectively. The efficiency of a PV device under the illumination of the

transmitted spectrum through the photoanode,  $\eta_{TS}$ , is determined by its  $MPP_{TS}$  divided by the average intensity of AM1.5:

$$\eta_{TS} = \frac{P_{MPP,TS}}{P_{Incident}} = \frac{V_{MPP,TS} \times J_{MPP,TS}}{100\text{mW}\cdot\text{cm}^{-2}} \times 100\% \quad (7)$$

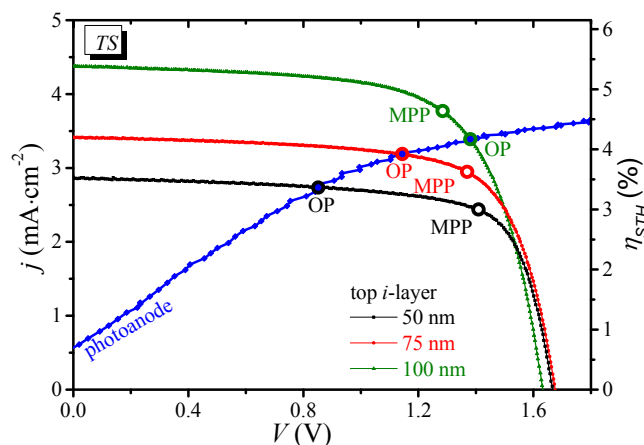


**Figure 6** The  $j$ - $V$  characteristics of the photoanode measured under the AM1.5 spectrum illumination (blue) and the  $j$ - $V$  characteristics corresponding to the three a-Si:H/a-Si:H double junction cells with various *i*-layer thickness measured under the illumination of the transmitted spectrum (TS) through the photoanode. The maximum power point (MPP) of the solar cells and the corresponding operating point (OP) in the PEC-WSDs are shown as well. The right axis reflects the corresponding  $\eta_{STH}$ .

The  $MPP_{TS}$  of the PV part of the PEC-WSD is in general not equal to the OP of the PEC-WSD. The loss due to the power mismatching between the OP (solid circles in Figure 6) and the  $MPP_{TS}$  (hollow circles in Figure 6) is defined as  $\Delta P = P_{OP} - P_{MPP,TS}$ . As shown by the green diamonds in Figure 5, the minimum mismatching loss is achieved for the PEC-WSD with the thick solar cell. This allows us to define an effective fill factor for the OP:

$$FF_{OP} = \frac{V_{OP} \times J_{OP}}{V_{OC,TS} \times J_{SC,TS}} \times 100\% \quad (8)$$

By comparing the OP and  $MPP_{TS}$  of each cell in Figure 6, the  $FF_{OP}$  of thick solar cell turns out to be the highest, as shown in Figure 5.

## 5. Performance and Stability of the PEC-WSD

In this section, we address the performance and the stability of the PEC cell and the PV cell of the PEC-WSD. First, we focus on the performance and the stability of the PEC part. The gradient-doped W:BiVO<sub>4</sub> PEC is connected to the optimized thick solar cell using a wire configurations as illustrated in Figure 1 (a).

The resulting chronoamperometry plot of this combined device is shown in Figure 7. In the first minute of the AM1.5 illumination, the  $J_{OP}$  of the PEC-WSD reaches  $\sim 4.2 \text{ mA}\cdot\text{cm}^{-2}$ , corresponding to  $\eta_{STH} \sim 5.2\%$ . This  $j$  value is slightly higher than the results shown in Figure 5 ( $\sim 3.4 \text{ mA}\cdot\text{cm}^{-2}$ ,  $\eta_{STH} \sim 4.2\%$ ). The main reason is that the potentiostat should sweep from the lower voltage to higher voltage in the  $j$ - $V$  curve measurement of the photoanode. In these few minutes, the generated  $\text{O}_2$  bubbles that accumulate on the surface of the photoanode reduce the number of active catalysts on the surface. This would result in a lower  $j$  value near the OP of photoanode (green solid circle in Figure 6) than the  $j$  value in the beginning moment of the stability measurement of the hybrid PEC-WSD. This initial decrease can be inferred in Figure 7 as well:  $j$  value drops and tends to stabilize at  $\sim 3.4 \text{ mA}\cdot\text{cm}^{-2}$  ( $\eta_{STH} \sim 4.2\%$ ) after  $\sim 2.5$  minutes in the measurement.

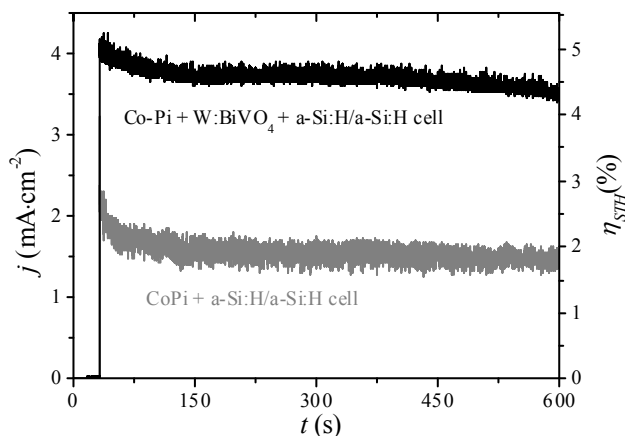


**Figure 7** Photocurrent density vs. time for the CoPi coated gradient-doped  $\text{W:BiVO}_4$  and double junction a-Si:H/a-Si:H device (black), and the CoPi-coated FTO/a-Si:H/a-Si:H device (grey) under AM1.5 illumination

Longer term reduction of the  $j$  might be due to the CoPi layer peeling off into the electrolyte. The  $\sim 4.2\%$  efficiency we report in this paper was determined after stabilizing for 10 minutes in the illuminated electrolyte. In addition, in a recent publication,<sup>30</sup> we demonstrated a stable  $4.9\%$   $\eta_{STH}$  by optimizing the  $\text{W:BiVO}_4$  photoanode and careful deposition of the CoPi layer. As a result, no degradation in the performance was observed during the course of one hour measurement. We achieve this highest efficiency for metal oxide semiconductor photoanode reported to date, using double junction a-Si:H solar cell which is cheaper and easier to fabricate as compared to triple junction solar cell used the benchmark structure reported in literature.<sup>36</sup> This  $4.9\%$  stable  $\eta_{STH}$  value is higher than the  $4.2\%$   $\eta_{STH}$  value we have achieved in this paper, and the reason for that is the difference of the substrate on the photoanode side. The  $4.9\%$   $\eta_{STH}$  was obtained by using a textured FTO coated glass (ASAHI VU-type) as the substrate of  $\text{BiVO}_4$ . In contrast, a flat FTO substrate (TEC-15) is used in this work, mainly because we are focusing on the optimization of the solar cell. Using a flat substrate, less light is being trapped in the

photoanode, and higher spectrum photon flux is available for the solar cell.

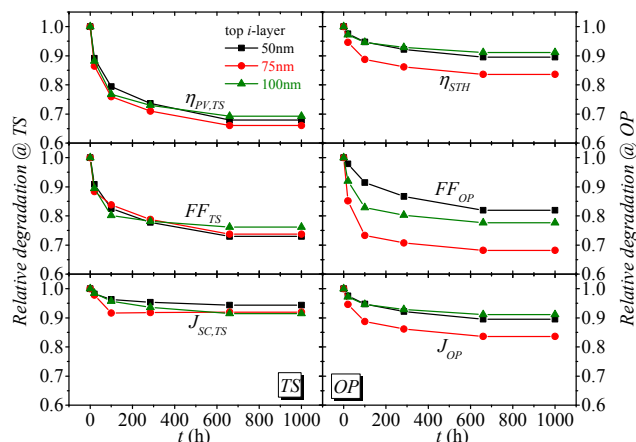
To illustrate the contribution of the gradient-doped  $\text{W:BiVO}_4$ , the  $\text{W:BiVO}_4$  photoanode is replaced by only an electrodeposited layer of CoPi on the same type of FTO substrate. As a result, only  $\sim 1.5 \text{ mA}\cdot\text{cm}^{-2}$  of photocurrent density is observed (grey curve in Figure 7), significantly lower than the gradient-doped  $\text{W:BiVO}_4$  photoanode. This confirms that the CoPi-based electrocatalyst requires significant higher bias voltages as delivered by a triple junction a-Si:H PV device, in order to obtain a reasonable  $\eta_{STH}$ . This demonstrates the advantage of the  $\text{BiVO}_4$  photoanode in reference to the CoPi-based electrocatalyst which provides a significant overpotential for water oxidation.

Finally, we discuss the stability of the PV part of the PEC-WSDs. The a-Si:H/a-Si:H tandem cell suffers from the SWE, which is the creation of additional metastable defects in the a-Si:H absorber layer when exposed to light. These metastable light induced defects enhance the charge carrier recombination and deteriorates the  $FF$  mainly and the  $J_{SC}$  of the a-Si:H solar cell to a less extent. The effect can be reversed by thermally annealing out the metastable defects at moderate temperatures of  $120$ - $180$  °C. The impact of the SWE metastability on the  $\eta_{STH}$  of the PEC-WSD is studied in the following paragraphs as well.

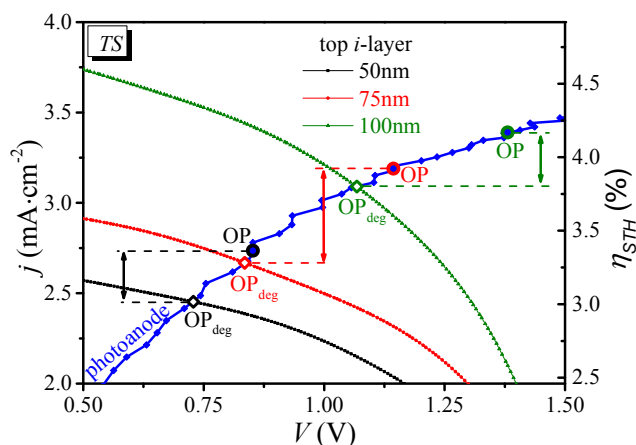
Light soaking experiments of the solely a-Si:H/a-Si:H devices were carried out under 1 Sun AM1.5 illumination, while keeping the solar cell at a temperature of  $25$  °C. The relative degradation of  $\eta_{TS}$ ,  $\eta_{STH}$ ,  $J_{SC,TS}$ ,  $J_{OP}$  and  $FF_{TS}$  measured versus light soaking time are illustrated in Figure 8 respectively. After light soaking of  $\sim 660$  h all three devices are fully degraded and stabilized. Among the external parameters, the  $FF$  shows the largest relative decrease after 1000 h illumination, i.e.  $\Delta FF_{TS}/FF_{TS}$  is 20-30% of the corresponding initial value. The relative degradation of the current density  $\Delta J_{SC,TS}/J_{SC,TS}$  and open circuit voltage  $\Delta V_{OC,TS}/V_{OC,TS}$  (not shown in Figure 8) is ranging from 5% up to 10%. As a result the relative decrease of the conversion efficiency  $\Delta \eta_{TS}/\eta_{TS}$  after stabilization is ranging from 30% up to 35%. Figure 8 demonstrates that the largest part of the degradation occurs in the first 20 hours of light soaking, which is in general addressed to as the ‘fast’ degradation phase. The ‘slow’ degradation phase corresponds to the additional slow degradation of external parameters after 20 hours of light soaking until the saturated external values for the external parameters are reached after 660 hours of light soaking.

Figure 8 shows that relative degradation of  $\eta_{STH}$  ranging from 9% up to 18% is significant smaller compared to  $\eta_{TS}$  ( $\sim 32\%$ ). This demonstrates the OP is less affected by SWE degradation than the  $\text{MPP}_{TS}$  of the PV part. Another observation is that the stabilized  $\eta_{STH}$  depends on the thickness of the top cell. As illustrated in Figure 9, this can be explained by the differences

in sensitivity of the OP to the degrading external parameters. If the slope ( $dj/dV$ ) of the  $j$ - $V$  curve of the photoanode in the OP is steep, the OP is more sensitive to degradation of  $J_{SC,TS}$ ,  $V_{OC,TS}$  and  $FF_{TS}$ . Whereas if the slope  $dj/dV$  of the  $j$ - $V$  curve is less steep (at higher voltages), OP becomes less sensitive to the degradation of the  $J_{SC,TC}$  as can be seen in Figure 9. The OP of thick solar cell has the highest voltage and consequently intersects the  $j$ - $V$  curve in a range with the smallest slope  $dj/dV$ . Therefore the PEC-WSD with the thick solar cells is less affected by the degradation in  $J_{SC,TS}$ . The OP of the PEC-WSD based on the thin solar cell has the smallest voltage and  $j$ - $V$  curve in a range with the largest slope  $dj/dV$ . Consequently, this PEC-WSD should be the most sensitive to variation in the  $J_{SC,TS}$ . However, since the degradation  $\Delta J_{SC,TS} / J_{SC,TS}$  is the smallest for thin solar cell, the effective drop in  $\eta_{STH}$  is the smallest. Therefore, the  $\eta_{STH}$  is a competition between the sensitivity of the changes of the external parameters given by the  $dj/dV$  at the OP and the degradation of the external parameters itself. For that reason, the PEC-WSD based on the medium solar cell shows the largest degradation in  $\eta_{STH}$  (red arrow in Figure 9). It is more sensitive to the degradation due to a larger slope  $dj/dV$  in reference to the PEC-WSD based on the thick solar cell, and also experience a larger degradation in  $J_{SC}$  in reference to PEC-WSD based on the thin solar cell. This effect is illustrated in Figure 9 as well.



**Figure 8** The relative degradation of the  $\eta$ ,  $FF$  and  $J_{SC}$  of the double junction PV cells with the light soaking time, normalized according to the as-deposited value of each device under the photoanode transmitted spectrum (TS) (left) and the operating point (OP), respectively.



**Figure 9** The  $j$ - $V$  characteristics of the three a-Si:H/a-Si:H double junction cells with various  $i$ -layer thickness after 1000 h light soaking and measured under the transmitted spectrum (TS) through the photoanode. The operating points of the degraded devices ( $OP_{deg}$ ) are indicated by the hollow circles on the inter-crossing points, and as a reference the operating point (OP) of the as-deposited PV cells are depicted by the solid circles with the corresponding colour (shown in Figure 6 as well).

## 6. Conclusion

CoPi-catalysed gradient-doped  $W:BiVO_4$ , deposited by spray pyrolysis, is confirmed as an efficient photoanode to split the water using solar energy. An a-Si:H tandem solar cell is introduced in order to provide the bias power source and is integrated into a wireless PEC-WSD. The advantage of the a-Si:H/a-Si:H double junction solar cell above other PV technologies is that it is simplest and cheapest PV device that can meet the requirement of stability in aqueous environments, straightforward fabrication process, matching spectral response, voltage and current.

Due to absorption of the  $W:BiVO_4$  photoanode in the front, only  $\sim 10\%$  of blue and  $\sim 60\%$  of red spectral range in the AM1.5 solar spectrum can be utilized by the a-Si:H/a-Si:H tandem cell. The thickness of the  $i$ -layer in the top cell has been optimized in term of current matching using both EQE measurements and ASA simulations. The thin solar cell ( $i$ -layer of 50 nm in top cell) shows the best current matching under AM1.5 spectrum, while the thick solar cell ( $i$ -layer of 100 nm in top cell) performs the best in reference to the spectrum transmitted through photoanode.

The impact of the Staebler-Wronski effect on the  $\eta_{STH}$  of the photoelectrochemical water splitting devices has been studied. The operating point is fortunately less affected by the SWE compared to the maximum power point of the solar cell component under the transmitted spectrum through the photoanode. The optimized a-Si:H/a-Si:H tandem solar cell combined with  $BiVO_4$  can result in a photocurrent of  $\sim 3.4$   $mA \cdot cm^{-2}$  (stabilize for 10 min), which corresponds to an  $\eta_{STH}$  of 4.2%.

The  $\eta_{STH}$  can be further enhanced provided that the infra-red range of the solar spectrum is better utilized, by using a double junction cell in which the bottom cell is based on PV materials with a lower bandgap, e.g., the micromorph (a-Si:H/nc-Si:H) solar cells. In addition, further optimization of the photoanode material and device is promising, which might reduce the high current and voltage requirement of the solar cell. Furthermore, by the implementation of some light trapping techniques at the photoanode, higher current density can be achieved due to absorption in the photoanode. The progress of going from concepts based on a triple junction solar cell to a double junction solar cell is already realized in this paper. Our next objective is to utilize a single junction solar cell in the PEC-WSD to reach higher values of the  $\eta_{STH}$ .

### Acknowledgements

The authors would like to thank the following PVMD colleagues: Pavel Babal and Marinus Fisher for the discussions in solar cell deposition; Dr. Serge Solntsev for the assistance in ASA simulation. Financial support from the VIDI project (granted to Dr. Arno H.M. Smets) by NWO-STW and European Commission's Framework Project 7 (NanoPEC, Project 227179) are gratefully acknowledged.

### Author contributions

L.H. and A.H.M.S. designed the tandem solar cell structure. L.H. synthesized, optimized and simulated the double junction a-Si:H solar cell. L.H. and P.P.R. finished the  $j$ - $V$  curve, EQE, light soaking measurements of the solar cell. F.F.A. and R.v.d.K. designed the homojunction concept of the photoanode. F.F.A. carried out BiVO<sub>4</sub> spray deposition and CoPi catalyst deposition. F.F.A. and L.H. measured the  $j$ - $V$  and the  $j$ - $t$  curve of the hybrid PEC-WSD. L.H. and A.H.M.S. wrote the draft. A.H.M.S., M.Z., B.D., and R.v.d.K. supervised the project. All the authors discussed the results and implications, and commented on the manuscript at all stages.

### Notes and references

<sup>a</sup> Photovoltaic Materials and Devices (PVMD) Laboratory, Delft University of Technology, P.O. Box 5031, 2600 GA Delft, Netherlands. Fax: +31 15 27 82968; Tel: +31 15 27 88906; \*E-mail: L.Han@tudelft.nl

<sup>b</sup> Materials for Energy Conversion and Storage (MECS) Laboratory, Delft University of Technology, P.O. Box 5045, 2600 GA Delft, Netherlands

<sup>c</sup> Helmholtz-Zentrum Berlin für Materialien und Energie GmbH, Institute for Solar Fuels, Hahn-Meitner-Platz 1, Berlin 14109, Germany

- F.F. Abdi, N. Firet and R. van de Krol, *ChemCatChem*, 2012, **5**, 490–496.
- W. Luo, Z. Yang, Z. Li, J. Zhang, J.Liu, Z. Zhao, Z. Wang, S. Yan, T. Yua and Z. Zou, *Energy Environ. Sci.*, 2011, **4**, 4046–4051.
- A. Kudo, K. Ueda, H. Kato, H. Kato and I. Mikami, *Catal. Lett.*, 1998, **53**, 229.
- A. Kudo, K. Omori and H. Kato, *J. Am. Chem. Soc.*, 1999, **121**, 11459–11467.
- F.F. Abdi, N. Firet, A. Dabirian and R. van de Krol, *MRS Online Proceedings Library*, 2012, **1446**, 10.1557.
- S. Tokunaga, H. Kato and A. Kudo, *Chem. Mater.*, 2001, **13**, 4624.
- P. Chatchai, Y. Murakami, S.Y. Kishioka, A.Y. Nosaka and Y. Nosaka, *Electrochem. Solid State Lett.*, 2008, **11**, H160–H163.
- S.P. Berglund, D.W. Flaherty, N.T. Hahn, A.J. Bard and C.B. Mullins, *J. Phys. Chem. C*, 2001, **115**, 3794.
- L.H. Dall'Antonia, N.R. de Tacconi, W. Chanmanee, H. Timmaji, N. Myung and K. Rajeshwar, *Electrochem Solid State Lett.*, 2010, **13**, D29–D32.
- M. Li, L. Zhao and L. Guo, *Int. J. Hydrogen Energy*, 2010, **35**, 7127–7133.
- M. Long, W. Cai and H. Kisch, *J. Phys. Chem. C*, 2008, **112**, 548–554.
- T. H. Jeon, W. Choi and H. Park, *Phys. Chem. Chem. Phys.*, 2011, **13**, 21392–21401.
- S.K. Pilli, T.E. Furtak, L.D. Brown, T.G. Deutsch, J.A. Turner and A.M. Herring, *Energy Environ. Sci.*, 2011, **4**, 5028–5034.
- S.K. Pilli, T.G. Deutsch, T.E. Furtak, J.A. Turner, L.D. Brown and A.M. Herring, *Phys. Chem. Chem. Phys.*, 2012, **14**, 7032–7039.
- K. Sayama, N. Wang, Y. Miseki, H. Kusama, N. Onozawa-Komatsuzaki and H. Sugihara, *Chem. Lett.*, 2010, **39**, 17–19.
- J. A. Seabold and K. S. Choi, *J. Am. Chem. Soc.*, 2012, **134**, 2186–2192.
- H. Ye, H. S. Park and A. J. Bard, *J. Phys. Chem. C*, 2011, **115**, 12464–12470.
- D. K. Zhong, S. Choi and D. R. Gamelin, *J. Am. Chem. Soc.*, 2011, **133**, 18370–18377.
- F. F. Abdi and R. van de Krol, *J. Phys. Chem. C*, 2012, **116**, 9398–9404.
- W. Hamd, S. Cobo, J. Fize, G. Baldinozzi, W. Schwartz, M. Reymermier, A. Pereira, M. Fontecave, V. Artero, C. Laberty-Robert and C. Sanchez, *Phys. Chem. Chem. Phys.*, 2012, **14**, 13224–13232.
- G.W. Ho, K.J. Chua and D.R. Siow, *J. Chem. Eng.*, 2012, **181–182**, 661–666.
- Y. Li, L. Zhang, A. Torres-Pardo, J.M. González-Calbet, Y. Ma, P. Oleynikov, O. Terasaki, S. Asahina, M. Shima, D. Cha, L. Zhao, K. Takanabe, J. Kubota and K. Domen, *Nature Commun.*, 2013, **4**, 2566.
- Z. Chen, T.F. Jaramillo, T.G. Deutsch, A. Kleiman-Shwarscstein, A.J. Forman, N. Gaillard, R. Garland, K. Takanabe, C. Heske, M. Sunkara, E.W. McFarland, K. Domen, E.L. Miller, J. A. Turner and H.N. Dinh, *J. Mater. Res.*, 2010, **25**, 3–16.
- M. Grätzel, *Nature*, 2001, **414**, 338–344.
- A.E. Delahoy, S.C. Gau, O. J. Murphy, M. Kapur and J.O. Bockris, *Int. J. Hydrogen Energy*, 1985, **10**, 113.
- E.L. Miller, R.E. Rocheleau and X.M. Deng, *Int. J. Hydrogen Energy*, 2003, **28**, 615.
- J. Brillet, J.H. Yum, M. Cornuz, T. Hisatomi, R. Solarska, J. Augustynski, M. Grätzel and K. Sivula, *Nature Photonics*, 2012, **6**, 824–828.
- O. Khaselev and J. A. Turner, *Science*, 1998, **280**, 425.
- S. Licht, B. Wang, S. Mukerji, T. Soga, M. Umeno and H. Tributsch, *J. Phys. Chem. B*, 2000, **104**, 8920–8924.
- F.F. Abdi, L. Han, A.H.M. Smets, M. Zeman, B. Dam and R. van de Krol, *Nature Commun.*, 2013, **4** (2195), 1–7.
- D.L. Staebler and C.R. Wronski, *Appl. Phys. Lett.*, 1977, **31**, 292.
- W. Theiss, *SCOUT Thin Film Analysis Software Handbook*, 2002 (Aachen).
- M. Zeman, J. van den Heuvel, M. Kroon, J. Willemen, B. Pieters, J. Krč and S. Solntsev, *Advance Semiconductor Analysis User Manual*, 2011 (Delft).
- T. Kirchartz, Generalized detailed balance theory of solar cells, 2009, **38**, 17 (Jülich).
- D.E. Scaife, *Solar Energy*, 1980, **25** (1), 41–54.
- S.Y. Reece, J.A. Hamel, K. Sung, T.D. Jarvi, A.J. Esswein, J.J.H. Pijpers and D.G. Nocera, *Science*, 2011, **334**, 645–648.